



This discussion paper is/has been under review for the journal Atmospheric Chemistry and Physics (ACP). Please refer to the corresponding final paper in ACP if available.

# The contribution of oceanic methyl iodide to stratospheric iodine

S. Tegtmeier<sup>1</sup>, K. Krüger<sup>1</sup>, B. Quack<sup>1</sup>, E. Atlas<sup>2</sup>, D. R. Blake<sup>3</sup>, H. Boenisch<sup>4</sup>,  
A. Engel<sup>4</sup>, H. Hepach<sup>1</sup>, R. Hossaini<sup>5</sup>, M. A. Navarro<sup>2</sup>, S. Raimund<sup>1</sup>, S. Sala<sup>4</sup>,  
Q. Shi<sup>1</sup>, and F. Ziska<sup>1</sup>

<sup>1</sup>GEOMAR Helmholtz Centre for Ocean Research Kiel, Kiel, Germany

<sup>2</sup>Rosenstiel School of Marine and Atmospheric Science, University of Miami, Miami, Florida, USA

<sup>3</sup>University of California, Irvine, USA

<sup>4</sup>Goethe University Frankfurt am Main, Frankfurt, Germany

<sup>5</sup>Institute for Climate and Atmospheric Science, School of Earth and Environment, University of Leeds, Leeds, UK

Received: 4 April 2013 – Accepted: 13 April 2013 – Published: 30 April 2013

Correspondence to: S. Tegtmeier (stegtmeier@geomar.de)

Published by Copernicus Publications on behalf of the European Geosciences Union.

## The contribution of oceanic methyl iodide to stratospheric iodine

S. Tegtmeier et al.

Title Page

Abstract

Introduction

Conclusions

References

Tables

Figures

⏪

⏩

◀

▶

Back

Close

Full Screen / Esc

Printer-friendly Version

Interactive Discussion

## Abstract

We investigate the contribution of oceanic methyl iodide ( $\text{CH}_3\text{I}$ ) to the stratospheric iodine budget. Based on  $\text{CH}_3\text{I}$  measurements during three tropical ship campaigns and the Lagrangian transport model FLEXPART we provide a detailed analysis of  $\text{CH}_3\text{I}$  transport from the ocean surface to the cold point in the upper tropical tropopause layer (TTL). While average oceanic emissions differ by less than 50 % from campaign to campaign, the measurements show much stronger variations within each campaign. A positive correlation between the oceanic  $\text{CH}_3\text{I}$  emissions and the efficiency of  $\text{CH}_3\text{I}$  troposphere–stratosphere transport has been identified for some cruise sections. The mechanism of strong horizontal surface winds triggering large emissions on the one hand and being associated with tropical convective systems, such as developing typhoons, on the other hand, could explain the identified correlations. As a result of the simultaneous occurrence of large  $\text{CH}_3\text{I}$  emissions and strong vertical uplift, localized maximum mixing ratios of 0.6 ppt  $\text{CH}_3\text{I}$  at the cold point have been determined for observed peak emissions during the SHIVA-Sonne campaign in the coastal West Pacific. The other two campaigns give considerable smaller maxima of 0.1 ppt  $\text{CH}_3\text{I}$  for the TransBrom campaign in the open West Pacific and 0.03 ppt for emissions from the coastal East Atlantic during the DRIVE campaign. In order to assess the representativeness of the large local mixing ratios we use climatological emission scenarios to derive global upper air estimates of  $\text{CH}_3\text{I}$  abundances. The model results are compared to available upper air measurements including data from the recent ATTREX and HIPPO2 aircraft campaigns. In the East Pacific region, the location of the available measurement campaigns in the upper TTL, the comparisons give a good agreement indicating that around 0.01 to 0.02 ppt of  $\text{CH}_3\text{I}$  enter the stratosphere. However, other tropical regions, which are subject to stronger convective activity show larger  $\text{CH}_3\text{I}$  entrainment, e.g., 0.08 ppt in the West Pacific. The strong variations in the geographical distribution of  $\text{CH}_3\text{I}$  entrainment suggest that currently available upper air measurements are not

## The contribution of oceanic methyl iodide to stratospheric iodine

S. Tegtmeier et al.

Title Page

Abstract

Introduction

Conclusions

References

Tables

Figures

⏪

⏩

◀

▶

Back

Close

Full Screen / Esc

Printer-friendly Version

Interactive Discussion



representative of global estimates and further campaigns will be necessary in order to better understand the CH<sub>3</sub>I contribution to stratospheric iodine.

## 1 Introduction

It is currently believed that organic iodine compounds are not important for stratospheric ozone chemistry as a result of their very short lifetimes which allow only small fractions of the emitted iodine to reach the stratosphere (Aschmann et al., 2009; Montzka and Reimann, 2011). Emissions of iodinated compounds from the ocean into the atmosphere and subsequent strongly localized vertical transport in convective systems determines if and how much of the short-lived iodinated gases reach the upper tropical tropopause layer (TTL) and lower stratosphere. Both processes are highly variable in time and space and reliable global estimates should, if possible, be derived from frequent upper air observations and from model studies based on high resolution emission maps. In case iodinated species reach the upper troposphere and lower stratosphere (UTLS) they might enhance ozone destruction due to the possible role of active iodine in rapid interhalogen reactions (Solomon et al., 1994).

Methyl iodide (CH<sub>3</sub>I) is an important carrier of iodine from the surface to the free troposphere where it plays an important role for ozone chemistry, oxidizing capacities and the formation of ultrafine aerosols particles (Chameides and Davis, 1980; Davis et al., 1996; McFiggans et al., 2000; O'Dowd et al., 2002; Saiz-Lopez et al., 2012; Vogt et al., 1999). CH<sub>3</sub>I is emitted mainly from the ocean where biological and nonbiological sources have been identified. While some studies report algae and phytoplankton as biological sources of oceanic CH<sub>3</sub>I (Hughes et al., 2011; Manley and Dastoor, 1987, 1988; Manley and de la Cuesta, 1997; Smythe-Wright et al., 2006) most studies suggest photochemical production in the surface ocean as the dominant mechanism (Butler et al., 2007; Chuck et al., 2005; Hoppel and Wallace, 1996; Moore and Zafiriou, 1994; Richter and Wallace, 2004; Yokouchi et al., 2008).

### The contribution of oceanic methyl iodide to stratospheric iodine

S. Tegtmeier et al.

Title Page

Abstract

Introduction

Conclusions

References

Tables

Figures

⏪

⏩

◀

▶

Back

Close

Full Screen / Esc

Printer-friendly Version

Interactive Discussion



## The contribution of oceanic methyl iodide to stratospheric iodine

S. Tegtmeier et al.

Title Page

Abstract

Introduction

Conclusions

References

Tables

Figures

⏪

⏩

◀

▶

Back

Close

Full Screen / Esc

Printer-friendly Version

Interactive Discussion

Global emission estimates are based on oceanic and atmospheric  $\text{CH}_3\text{I}$  concentrations obtained during ship cruises (*bottom-up*) and on model studies which are adjusted to  $\text{CH}_3\text{I}$  upper-air observations (*top-down*) (Montzka and Reimann, 2011). Oceanic and atmospheric surface  $\text{CH}_3\text{I}$  is characterized by a large spatial (e.g., Ziska et al., 2013) and temporal (e.g., Fuhlbrügge et al., 2012) variability. Additionally, differences between calibration scales, applied during past campaigns, might exist (Butler et al., 2007). Estimating local fluxes from observations and extrapolating them to a larger scale in order to derive global estimates may thus result in large uncertainties. Atmospheric modeling studies on the other hand prescribe global emissions with the emission strength chosen so as to reproduce atmospheric aircraft observations and might miss the importance of localized sources. As a result emissions are poorly constrained and available global oceanic flux estimates based on the different approaches (top-down, bottom up and laboratory experiments) range widely from 180 to  $1163 \text{ Gg I yr}^{-1}$ . An overview of available global oceanic emission estimates in the literature is given in Table 1 in  $\text{Gg I yr}^{-1}$  and, for a better comparability to the ship campaign emissions presented in Sect. 3, in  $\text{pmol CH}_3\text{I m}^{-2} \text{ h}^{-1}$ . Additionally, terrestrial sources such as rice paddies, wetlands, and biomass burning, which are not well quantified yet, are assumed to contribute 80–110  $\text{Gg I yr}^{-1}$  (Bell et al., 2002; Redeker et al., 2000; Sive et al., 2007).

Atmospheric mixing ratios of  $\text{CH}_3\text{I}$  in the marine boundary layer have been reported from a large number of measurement campaigns and background values range between 0.4 and 1.6 ppt (Saiz-Lopez et al., 2012 and references therein). With increasing altitude the  $\text{CH}_3\text{I}$  abundance decreases and measurements from two aircraft campaigns reveal very little  $\text{CH}_3\text{I}$  in the TTL with mean values of 0.01 ppt above 14 km (Montzka and Reimann, 2011). The two campaigns have been conducted with the NASA WB57 high-altitude aircraft over Central America and the Gulf of Mexico and, due to the horizontal limitations of the campaign area, the results might not be representative of global  $\text{CH}_3\text{I}$  estimates in the TTL. The observational data obtained during the aircraft campaigns combined with the outcome of model studies (Aschmann et al.,

## The contribution of oceanic methyl iodide to stratospheric iodine

S. Tegtmeier et al.

Title Page

Abstract

Introduction

Conclusions

References

Tables

Figures

⏪

⏩

◀

▶

Back

Close

Full Screen / Esc

Printer-friendly Version

Interactive Discussion

2009; Donner et al., 2007; Gettelman et al., 2009) lead to the conclusion that no more than 0.05 ppt of iodine enters the stratosphere as the source gas  $\text{CH}_3\text{I}$  before being photolyzed (Montzka and Reimann, 2011). Once in the lower stratosphere  $\text{CH}_3\text{I}$  will contribute to the inorganic iodine ( $I_y$ ) budget which is of interest due to the suggested efficiency of active iodine in destroying ozone (Davis et al., 1996; Solomon et al., 1994; WMO, 2007). Investigations of inorganic iodine species, in the form of iodine monoxide (IO) or iodine dioxide (OIO), in the lower stratosphere reveal only undetectably low amounts. As a result the total amount of stratospheric  $I_y$  is estimated to be below 0.15 ppt (Montzka and Reimann et al., 2011) arising from the detection limit of inorganic iodine (0.1 ppt) and the iodine supply in form of  $\text{CH}_3\text{I}$  (0.05 ppt).

Due to its short lifetime of around 7 days (given in Montzka and Reimann et al., 2011) one expects  $\text{CH}_3\text{I}$  in the troposphere and TTL to exhibit significantly large variability. The amount of  $\text{CH}_3\text{I}$  transported from the ocean into the stratosphere is determined by oceanic emissions and the efficiency of atmospheric transport. In order to quantify the contribution of  $\text{CH}_3\text{I}$  to the stratospheric  $I_y$  budget observations of  $\text{CH}_3\text{I}$  and IO with a good global coverage would be necessary. Such observational evidence of global upper air iodine abundances does not exist so far. However, a variety of  $\text{CH}_3\text{I}$  surface data originating from ship campaigns as well as the thereby generated first global emission climatology (Ziska et al., 2013) are available. Here, we use in-situ  $\text{CH}_3\text{I}$  measurements from three tropical ship campaigns, one in the East Atlantic and two in the West Pacific, and a Lagrangian transport model to analyze the characteristics and the variability of  $\text{CH}_3\text{I}$  transport from the ocean surface into the upper TTL. Furthermore we derive upper air estimates of  $\text{CH}_3\text{I}$  abundances based on the global emission climatology and compare them to available upper air measurements including new data from various aircraft campaigns. The ship and aircraft campaigns as well as the atmospheric transport model are introduced in Sect. 2. Estimates of atmospheric  $\text{CH}_3\text{I}$  abundances based on the individual ship campaigns are given in Sect. 3, while the model results based on global emissions, including their comparisons to aircraft campaign data, are



## The contribution of oceanic methyl iodide to stratospheric iodine

S. Tegtmeier et al.

Title Page

Abstract

Introduction

Conclusions

References

Tables

Figures

⏪

⏩

◀

▶

Back

Close

Full Screen / Esc

Printer-friendly Version

Interactive Discussion



respectively. Note that SHIVA is a combined aircraft, ship and ground based campaign with both, measurements from the ship and from the aircraft, used in this study. From the HIPPO mission we use here the measurements obtained during the HIPPO2 campaign in 2009. CH<sub>3</sub>I measurements in the upper TTL are available from Pre-AVE and TC4 campaigns. These two campaigns have been used to derive recent estimates of the upper air CH<sub>3</sub>I abundance (Montzka and Reimann et al., 2011). In addition to the data used for the current upper TTL CH<sub>3</sub>I estimate, observations from the ACCENT campaign in 1999 and from the ATTREX campaign in 2011 are included in our study. All four campaigns, which provide CH<sub>3</sub>I measurements in the upper TTL, took place over the Southern US and Central America. Detailed information about the aircraft missions including location and time period are presented in Table 3.

### 2.3 Global emission climatology

The global emission scenario from Ziska et al. (2013) is a bottom-up estimate of the oceanic CH<sub>3</sub>I fluxes. Atmospheric and oceanic surface in-situ measurements from the HalOcat (Halocarbons in the ocean and atmosphere) database project (<https://halocat.geomar.de>) were used to generate global surface concentration maps. In a first step the surface measurements were classified based on physical and biogeochemical characteristics of the ocean and atmosphere important for the CH<sub>3</sub>I distribution and sources. Within each classified region the global 1° × 1° grid was filled through the extrapolation of the in-situ measurements based on the Ordinary Least Square (OLS) regression technique. The estimated surface concentration maps do not provide any information on temporal variability, but represent climatological fields of a 20 yr long time period. Based on the global concentration maps the oceanic emissions were calculated with the transfer coefficient parameterization of Nightingale et al. (2000), adapted to CH<sub>3</sub>I. The emission parameterization is based on 6 hourly meteorological ERA-Interim data (Dee et al., 2011) taking into account emission peaks related to maxima in the horizontal wind fields. The final emission climatology product is calculated as the 20 yr-average emission field. Emission peaks related to 6 hourly wind maxima are

not present any more in the final 20 yr mean climatology, however, their existence in the temporally resolved emission fields counteracts a possible underestimation introduced by smoothing effects of the climatological approach.

## 2.4 Modeling atmospheric transport

5 The atmospheric transport of CH<sub>3</sub>I from the oceanic surface into the upper troposphere and TTL is simulated with the Lagrangian particle dispersion model FLEXPART (Stohl et al., 2005). This model has been validated based on comparisons with measurement data from three large-scale tracer experiments (Stohl et al., 1998) and on intercontinental air pollution transport studies (e.g., Forster et al., 2001; Spichtinger et al., 2001; 10 Stohl and Trickl, 1999). FLEXPART is driven by meteorological fields from the ECMWF (European Centre for Medium-Range Weather Forecasts) numerical weather prediction model and includes parameterizations for moist convection (Forster et al., 2007), turbulence in the boundary layer and free troposphere (Stohl and Thomson, 1999), dry deposition and in-cloud as well as below-cloud scavenging, and the simulation of chemical decay. 15

In the present study we perform two different kind of studies based on the different model set ups, one using in-situ emissions observed during individual ship campaigns and one using a global emission climatology. For the in-situ experiments, the transport of CH<sub>3</sub>I is simulated with a multitude of trajectories launched for each emission data point, as described in detail by Tegtmeier et al. (2012). The trajectories are assigned the amounts of CH<sub>3</sub>I emitted from a 0.0002° × 0.0002° grid box (~ 500 m<sup>2</sup>) at the measurement location over one hour as calculated from the observation-derived flux. Atmospheric mixing ratio profiles resulting from in-situ emissions have been determined following the method described in Tegtmeier et al. (2012). The calculation of 20 global CH<sub>3</sub>I estimates is based on the emission climatology from Ziska et al. (2013). The oceanic sea-to-air flux is given globally on a 1° × 1° grid. From each grid box 10 trajectories are released per day carrying the according amount of CH<sub>3</sub>I as prescribed by the emission scenario. While the simulations based on the in-situ ship campaign 25

### The contribution of oceanic methyl iodide to stratospheric iodine

S. Tegtmeier et al.

Title Page

Abstract

Introduction

Conclusions

References

Tables

Figures

⏪

⏩

◀

▶

Back

Close

Full Screen / Esc

Printer-friendly Version

Interactive Discussion



## The contribution of oceanic methyl iodide to stratospheric iodine

S. Tegtmeier et al.

Title Page

Abstract

Introduction

Conclusions

References

Tables

Figures

⏪

⏩

◀

▶

Back

Close

Full Screen / Esc

Printer-friendly Version

Interactive Discussion

data are carried out for the time period of the respective ship campaigns (see Table 2), the global simulations are run for the year 2009. Additionally, the global simulations are carried out for the time periods of the aircraft campaigns (see Table 3) in order to allow for a direct comparison between aircraft measurements and model results.

The FLEXPART runs are driven by the ECMWF reanalysis product ERA-Interim (Dee et al., 2011) given at a horizontal resolution of  $1^\circ \times 1^\circ$  on 60 model levels. Transport, dispersion and convection of the air parcels are calculated from the 6-hourly fields of horizontal and vertical wind, temperature, specific humidity, convective and large scale precipitation and others. A pre-processor retrieves the meteorological fields from the ECMWF archives, including the vertical wind which is calculated in hybrid coordinates mass-consistently from spectral data.

The atmospheric lifetime of  $\text{CH}_3\text{I}$  was assumed to be constant in the troposphere and set to 7 days according to current estimates (Montzka and Reimann, 2011). Trajectories were terminated after 20 days. For a sensitivity study, an altitude-dependent lifetime of  $\text{CH}_3\text{I}$ , derived by the TOMCAT chemical transport model (CTM) (Chipperfield, 2006), was also used. The CTM calculated tropospheric loss of  $\text{CH}_3\text{I}$  through photolysis, the major tropospheric sink, using the recommended absorption cross section data of Sander et al. (2011). The modeled  $\text{CH}_3\text{I}$  lifetime diagnosed by the CTM is relatively short ( $\sim 2\text{--}3$  days) in the tropical troposphere and thus this experiment is useful to examine the sensitivity of  $\text{CH}_3\text{I}$  loading in the upper troposphere to a range of lifetimes. Previously,  $\text{CH}_3\text{I}$  profiles from TOMCAT have been shown to agree well with aircraft observations in the tropical troposphere (Hossaini et al., 2012). The mass of the  $\text{CH}_3\text{I}$  carried by each air parcel is reduced at a rate corresponding to its chemical lifetime.

### 3 Atmospheric CH<sub>3</sub>I transport based on individual ship campaigns

#### 3.1 Comparison of three tropical campaigns

CH<sub>3</sub>I emissions observed during the tropical ship cruises vary substantially from campaign to campaign. Figure 2a shows the campaign-averaged emissions for all three cruises, with stronger emissions for the coastal West Pacific campaign SHIVA-Sonne (referred to as SHIVA hereinafter) compared to the North East Atlantic campaign DRIVE and the open West Pacific campaign TransBrom-Sonne (referred to as TransBrom hereinafter). In contrast to global estimates (Table 1), the emissions observed during the three campaigns are small with mean values of 310 (DRIVE), 320 (TransBrom) and 430 (SHIVA) pmolm<sup>-2</sup>h<sup>-1</sup> just below the minimum global estimate (443 pmolm<sup>-2</sup>h<sup>-1</sup>, Chuck et al., 2005) and three times smaller than the maximum global estimate (1354 pmolm<sup>-2</sup>h<sup>-1</sup>, Butler et al., 2007).

Black lines in Fig. 2b–d give the emission strength along the cruise tracks and demonstrate the large variability of sea-to-air fluxes during the campaigns with the measurement locations often about less than 100 km apart from each other. CH<sub>3</sub>I is generally oversaturated in oceanic surface waters. As a result, emission flux is primarily controlled by concentrations in water (rather than air) and the water-air exchange rate, which is in turn driven by the wind speed (Ziska et al., 2013). In addition to the emission time series the wind speed along the cruise track (colored dashed lines) for the individual campaigns is presented in Fig. 2b–d. Particularly high emissions occur for the TransBrom cruise during times of high wind speeds, e.g., emissions of up to 1364 and 600 pmolm<sup>-2</sup>h<sup>-1</sup> were observed during the tropical storms Nepartak and Lupit on 12 October and 14 October 2009, respectively (Quack et al., 2013). CH<sub>3</sub>I emissions during the DRIVE campaign are also determined by the large supersaturation in combination with varying wind speeds and the largest emissions of up to 1146 pmolm<sup>-2</sup>h<sup>-1</sup> have been observed on 7 June 2010. For SHIVA relatively high oceanic concentrations and warm water temperatures lead to very high supersaturations of methyl iodide in the coastal West Pacific and trigger large CH<sub>3</sub>I emissions due to elevated wind speeds.

## The contribution of oceanic methyl iodide to stratospheric iodine

S. Tegtmeier et al.

Title Page

Abstract

Introduction

Conclusions

References

Tables

Figures

⏪

⏩

◀

▶

Back

Close

Full Screen / Esc

Printer-friendly Version

Interactive Discussion



Local peak emissions during SHIVA of up to  $2980 \text{ pmol m}^{-2} \text{ h}^{-1}$  (19 November 2011) exceed the maximum emissions observed during the other two campaigns and are among the largest local emissions observed so far (Ziska et al., 2013).

The amount of  $\text{CH}_3\text{I}$  which reaches the stratosphere has been estimated based on Lagrangian transport calculations with FLEXPART.  $\text{CH}_3\text{I}$  emissions in the FLEXPART runs are calculated from the observed flux for a time period of one hour and an area of  $500 \text{ m}^2$  for each observation and are given in Fig. 3 as campaign averages (Fig. 3a) and as time series over the length of each individual campaign (Fig. 3b–d). The level above which no significant washout is expected is particularly important for stratospheric iodine chemistry, since all  $\text{CH}_3\text{I}$  which reaches this level before being photolyzed can be expected to contribute to the stratospheric  $\text{I}_y$  budget. While the exact altitude of the “no-washout level” is still under debate (Fueglistaler et al., 2009) we have chosen the cold point altitude as an upper estimate since no dehydration is expected to occur above. Based on evaluations of regular radiosonde measurements during the ship campaigns the cold point is found at 17 km (Fuhlbrügge et al., 2012; Krüger and Quack, 2012). We quantify the contribution of  $\text{CH}_3\text{I}$  to stratospheric iodine based on the amount of  $\text{CH}_3\text{I}$  entrained above 17 km, which is calculated as the sum of  $\text{CH}_3\text{I}$  carried by all the computational particles across this altitude. Note that the altitude of the level above which no wash-out occurs is a source of uncertainty regarding our results of the  $\text{CH}_3\text{I}$  contribution to stratospheric iodine. If, for instance, heterogeneous recycling of iodine from aerosols back to the gas phase would occur (Dix et al., 2013), the “no-washout level” would be lower than the cold point and, as a consequence, the  $\text{CH}_3\text{I}$  contribution to stratospheric iodine would be larger than estimated below. A simple sensitivity study reveals that approximately twice as much  $\text{CH}_3\text{I}$  is found to contribute to the stratospheric iodine if the “no-washout level” would be at 16 km instead of 17 km.

For all three campaigns the average amount of  $\text{CH}_3\text{I}$  being entrained above 17 km is shown in Fig. 3a. For the scenario of a uniform atmospheric lifetime of 7 days (WMO, 2011) about 0.5 % (DRIVE), 2 % (TransBrom) and 6 % (SHIVA) of the emitted  $\text{CH}_3\text{I}$  reaches the upper TTL and is projected to be entrained into the stratosphere. In order

## The contribution of oceanic methyl iodide to stratospheric iodine

S. Tegtmeier et al.

Title Page

Abstract

Introduction

Conclusions

References

Tables

Figures

⏪

⏩

◀

▶

Back

Close

Full Screen / Esc

Printer-friendly Version

Interactive Discussion

## The contribution of oceanic methyl iodide to stratospheric iodine

S. Tegtmeier et al.

Title Page

Abstract

Introduction

Conclusions

References

Tables

Figures

⏪

⏩

◀

▶

Back

Close

Full Screen / Esc

Printer-friendly Version

Interactive Discussion

to investigate the sensitivity of our results to the prescribed atmospheric lifetime of  $\text{CH}_3\text{I}$  we repeat the same calculation but using an altitude dependent  $\text{CH}_3\text{I}$  lifetime from the TOMCAT CTM. In case the considerable shorter profile lifetime (2 ~ 3 days) is assumed only 0.1 % (DRIVE), 1 % (TransBrom) and 4 % (SHIVA) of the emitted  $\text{CH}_3\text{I}$  are transported into the upper TTL. The entrainment of  $\text{CH}_3\text{I}$  above 17 km based on the two different lifetimes reveals considerable differences as one would expect and illustrates the need for a better understanding of tropospheric  $\text{CH}_3\text{I}$  chemistry. While all the following results are based on assuming a  $\text{CH}_3\text{I}$  atmospheric lifetime of 7 days, the case study above provides an estimate of the sensitivity of our results (30–80 % less entrainment) to variations of the atmospheric lifetime (2.5 ~ 3 days instead of 7 days).

The efficiency of atmospheric  $\text{CH}_3\text{I}$  transport from the surface to the cold point (given by the percentage value of  $\text{CH}_3\text{I}$  reaching 17 km) during SHIVA (West Pacific) is 12 to 40 times larger than the efficiency of  $\text{CH}_3\text{I}$  transport during DRIVE (Atlantic). While these results are derived from model runs based on local campaign data, it is known from previous studies that the West Pacific is in general an important region for troposphere–stratosphere transport of short-lived compounds (e.g., Aschmann et al., 2009; Krüger et al., 2009; Levine et al., 2007) due to active deep convection (Fueglistaler et al., 2009 and references therein). For SHIVA the large emissions together with the very efficient vertical transport lead to an overall large amount of  $\text{CH}_3\text{I}$  reaching the stratosphere. The absolute amounts of  $\text{CH}_3\text{I}$  being entrained above the cold point at 17 km are given in Fig. 3a for all campaigns, illustrating that 20 times more  $\text{CH}_3\text{I}$  is entrained for SHIVA when compared to DRIVE and 4 times more when compared to TransBrom.

### 3.2 Possible connection between $\text{CH}_3\text{I}$ emissions and atmospheric transport

Oceanic emissions and atmospheric transport vary from campaign to campaign but also considerably within each campaign. Dotted lines in Fig. 3b–d give the transport efficiency along the cruise track and demonstrate its large variability from measurement side to measurement side. During DRIVE the  $\text{CH}_3\text{I}$  troposphere–stratosphere transport

## The contribution of oceanic methyl iodide to stratospheric iodine

S. Tegtmeier et al.

Title Page

Abstract

Introduction

Conclusions

References

Tables

Figures

⏪

⏩

◀

▶

Back

Close

Full Screen / Esc

Printer-friendly Version

Interactive Discussion

is weak for the whole campaign and less than 1 % reaches the stratosphere (Fig. 3c). However, for the two West Pacific campaigns the vertical transport is more efficient lifting 1–16 % (0–6 %) of emitted  $\text{CH}_3\text{I}$  from the surface to 17 km for SHIVA (TransBrom). While both ship campaigns took place in the Western Pacific and encountered periods of strong convective activity the amount of overshooting convection, responsible for the transport of the short-lived  $\text{CH}_3\text{I}$  up to 17 km, differs between the campaigns. An overall stronger vertical transport is predicted for the SHIVA campaign which took place in the coastal regions of the maritime continent, an area well known for deep cumulus convection and heavy precipitation systems during boreal winter (Chang et al., 2005). For TransBrom, convection above the open ocean including tropical storm systems dominates the vertical transport from the surface to the cold point at 17 km. The total amount of  $\text{CH}_3\text{I}$  entrained above 17 km shows maximum values for cases when both emission and transport efficiency are large. For the SHIVA campaign, this coincidence is found for the event of the second largest emission on 22 November 2011 where the transport model estimates that around 10 %  $\text{CH}_3\text{I}$  could reach 17 km. For TransBrom, the largest total entrainment takes place on 14 October 2009 and is based on an average emission value during times of maximum efficiency of vertical transport.

In order to further analyze possible coincidences of strong emissions and efficient vertical transport a correlation analysis has been applied to the two time series. For the complete time series covering the whole cruise length no correlation exists for any of the three campaigns. However, if parts of the time series are analyzed high correlations are found. For the TransBrom campaign, correlations between emissions and vertical atmospheric transport maximize for two individual campaign sections (Fig. 4a). A very high correlation of 0.89 is found for the first section comprising 16 data points collected over 2 days (red lines). A high correlation ( $r = 0.69$ ) also exists for the subsequent cruise section extending from 13 October 2009 to 18 October 2009 based on 39 data points. All correlation coefficients are statistically significant at the 95 % confidence level based on the Student's  $t$  test. Scatter plots of the emissions versus vertical

atmospheric transport show different relationships for the two periods, with linear fits resulting in slopes of 54 and 5, respectively.

Understanding the two different regimes occurring during TransBrom, which show correlations if analyzed separately, but lead to non-correlated data sets when combined, requires some background information on the meteorological situation during the cruise (Krüger and Quack, 2012). The first cruise section extends north of the Inter Tropical Convergence Zone (ITCZ) from 32° N to 24° N and model results suggests that vertical transport from the surface to 17 km is weak with less than 1 % of CH<sub>3</sub>I being lifted by deep convection into the upper TTL. At the end of the first cruise section (12 October 2009, 27° N) the ship crossed the track of the tropical storm Nepartak and large horizontal wind speeds were observed reaching values of 20.4 ms<sup>-1</sup>. Measurements were increased to an hourly frequency and peak emissions of oceanic CH<sub>3</sub>I were reported during periods of maximum horizontal winds. Note that during the influence of Nepartak the transport model shows strong convective activity, however reaching only main convective outflow regions around 12 km and not the upper TTL, resulting in the weak transport efficiency discussed above. At the beginning of the second cruise section the ship crossed the ITCZ and came close to the tropical storm Lupit (14 October 2009, 18° N), which developed into a super typhoon a couple of days later (Krüger and Quack, 2012). Similar to the situation during Nepartak, the strong horizontal wind speeds are accompanied by increased atmospheric trace gas distributions and emissions. As opposed to the first cruise track section, atmospheric transport into the upper TTL is very efficient during the second cruise section in accordance with its location within the ITCZ.

For the SHIVA campaign, the correlation between oceanic emissions and atmospheric transport maximizes for the cruise section in the South China Sea from 17 November to 23 November 2011 comprising 47 data points. Figure 4b shows the two time series, oceanic emissions and troposphere–stratosphere transport efficiency, with the data during the respective cruise section displayed in red. The correlation ( $r = 0.59$ ) results mostly from the fact that the large emissions on 21–22 November 2011 are

**The contribution of oceanic methyl iodide to stratospheric iodine**

S. Tegtmeier et al.

Title Page

Abstract

Introduction

Conclusions

References

Tables

Figures

⏪

⏩

◀

▶

Back

Close

Full Screen / Esc

Printer-friendly Version

Interactive Discussion



---

**The contribution of oceanic methyl iodide to stratospheric iodine**S. Tegtmeier et al.

---

[Title Page](#)[Abstract](#)[Introduction](#)[Conclusions](#)[References](#)[Tables](#)[Figures](#)[⏪](#)[⏩](#)[◀](#)[▶](#)[Back](#)[Close](#)[Full Screen / Esc](#)[Printer-friendly Version](#)[Interactive Discussion](#)

5 accompanied by fast vertical transport. Note that for these two days high horizontal wind speeds of up to  $13 \text{ ms}^{-1}$  occurred, while the horizontal winds during the time period before were moderate around  $5 \text{ ms}^{-1}$ . After 23 November 2011 the horizontal winds and also the vertical transport continue to be large, however, due to lower oceanic concentrations and saturation anomalies the emissions are small compared with the first cruise section.

10 Based on two tropical campaigns in the West Pacific three cruise sections have been identified which show a correlation between the amount of  $\text{CH}_3\text{I}$  emitted from the ocean and the fraction of emitted  $\text{CH}_3\text{I}$  transported from the surface to the cold point at 17 km. In general,  $\text{CH}_3\text{I}$  shows relatively uniform oceanic concentrations over the various cruise sections (Quack et al., 2013). Emission rates are mainly determined by the wind speed variations with high wind speeds resulting in a fast atmospheric outflow and an immediate replacement of the gas from the oceanic source. Such correlations between emissions and horizontal wind speeds have also been observed for other short-lived halogenated gases such as  $\text{CHBr}_3$  and  $\text{CH}_2\text{Br}_3$  in supersaturated coastal waters during tropical storm activities (Zhou et al., 2008). We find the strongest  $\text{CH}_3\text{I}$  emissions during tropical storms which on the other hand can lead to intense vertical transport associated with developing tropical cyclones. It has been suggested that tropical cyclones could play an important role for troposphere–stratosphere exchange due to associated frequent convective overshooting (Rossow and Pearl, 2007) and due to contributing a disproportional large amount of the convection that penetrates the stratosphere (Romps and Kuang, 2009). The mechanism of strong horizontal winds triggering large emissions on the one hand and being associated with tropical convective systems on the other hand could provide a possible explanation of the identified correlations. Such a mechanism could also explain why data over longer time periods is uncorrelated if the meteorological or oceanic regime changes. Examples are the change in oceanic  $\text{CH}_3\text{I}$  concentration gradients during SHIVA on 23 November 2011 coinciding with the end of the correlation time period and the change of meteorological

15  
20  
25

conditions during TransBrom on 14 October, when crossing the ITCZ, coinciding with the switch between the two correlation regimes.

Correlation coefficients between all three quantities are presented in Table 4 for different sections of the two cruises. Evidently, in all cases there is a strong correlation between  $\text{CH}_3\text{I}$  emissions and the horizontal wind speed. In case the horizontal surface wind is also strongly correlated with the efficiency of vertical transport, we find the above discussed correlation between  $\text{CH}_3\text{I}$  emissions and vertical transport. The fact that for these cases both quantities are highly correlated with the horizontal wind further strengthens the above suggested mechanism. For the complete TransBrom cruise no correlation of the horizontal winds with the vertical transport can be found likely related to very different meteorological regimes. For the complete SHIVA campaign the correlation between  $\text{CH}_3\text{I}$  emission and horizontal winds is somewhat weaker than for the other cases likely related to a switch in the oceanic regime.

For the cruise sections where a correlation between emission and vertical transport could be identified, one also finds the overall largest amounts of  $\text{CH}_3\text{I}$  being transported into the stratosphere. For TransBrom the maximum amount of 0.1 ppt  $\text{CH}_3\text{I}$  at 17 km (Fig. 5) is associated with emissions on 14 October 2009 and subsequent atmospheric transport influenced by the tropical storm Lupit. Atmospheric  $\text{CH}_3\text{I}$  abundance at 17 km averaged over the whole campaign amounts to 0.02 ppt. During SHIVA very large peak emissions as well as very intense vertical transport result in model estimates of 0.6 ppt  $\text{CH}_3\text{I}$  at 17 km (Fig. 5) which is much larger than any values reported by high reaching aircraft measurements so far (Montzka and Reimann, 2011). The campaign average mixing ratio at 17 km is considerably lower amounting to 0.07 ppt. During DRIVE the maximum values at 17 km range around 0.03 ppt and mean values are in the order of 0.01 ppt (Fig. 5). In order to investigate whether the relatively large mixing ratios estimated for the West Pacific emissions are isolated cases strongly deviating from otherwise low  $\text{CH}_3\text{I}$  abundances or if they occur frequently enough to impact global  $\text{CH}_3\text{I}$  in the upper TTL, we analyze global model runs in Sect. 4.

**The contribution of oceanic methyl iodide to stratospheric iodine**

S. Tegtmeier et al.

Title Page

Abstract

Introduction

Conclusions

References

Tables

Figures



Back

Close

Full Screen / Esc

Printer-friendly Version

Interactive Discussion





deviation over all coincidences identified for the particular campaign data and for the corresponding model output.

The profile comparison for the three aircraft campaigns, which provide data in the free troposphere and lower UTLS, show in general a good agreement between the observations and the model results with the latter being consistently lower (Fig. 7). For TC4-DC8, the modeled profile shows a steeper vertical gradient between 1 and 3 km than the observations leading to some disagreement below 5 km. Above this level model output and observations agree within their respective standard deviations. The HIPPO2 flight tracks extend over all tropical latitudes and campaign averaged profiles show a large variability below 10 km and around 13–14 km, which is also displayed although somewhat weaker by the model results. Mean values agree very well on some levels (e.g., above 10 km) but show larger discrepancies on other levels (e.g., 3–4 km). For SHIVA, the variability over all flight sections is small for observations and model results. In general, observed and modeled profiles show a very similar shape with FLEXPART results being slightly smaller consistently over the whole altitude range. The largest differences are found around 11 km. For some individual flights convective outflow leads to observations of enhanced  $\text{CH}_3\text{I}$  between 10 and 12 km resulting in a “C-shape” profile (Sala et al., 2013) a characteristic which is well captured by the model results (not shown here).

## 4.2 Comparison with aircraft measurements in the upper TTL

Model-measurement comparisons for the four campaigns conducted with the high-altitude aircraft sampling in the upper TTL and lower stratosphere are shown in Fig. 8. For three out of four campaigns the modeled abundances above 10 km agree very well with the observations. For all three cases the mixing ratios in the upper TTL are below 0.1 ppt with the exception of the strongly enhanced mixing ratios at 16 km during ACCENT, which are reported by the observations and the model results. Largest discrepancies are found for the TC4-WB57 campaign where basically no  $\text{CH}_3\text{I}$  was observed above 15 km while FLEXPART simulates mixing ratios around 0.1 ppt for the

### The contribution of oceanic methyl iodide to stratospheric iodine

S. Tegtmeier et al.

Title Page

Abstract

Introduction

Conclusions

References

Tables

Figures

⏪

⏩

◀

▶

Back

Close

Full Screen / Esc

Printer-friendly Version

Interactive Discussion



## The contribution of oceanic methyl iodide to stratospheric iodine

S. Tegtmeier et al.

Title Page

Abstract

Introduction

Conclusions

References

Tables

Figures

⏪

⏩

◀

▶

Back

Close

Full Screen / Esc

Printer-friendly Version

Interactive Discussion

levels 13–17 km. Only below 10 and above 17 km the model output agrees well with the TC4-WB57 observations. A summary of the model-measurement comparison in the TTL is displayed in Fig. 9 where the modeled and observed profiles averaged over all four campaigns are displayed. FLEXPART overestimates the amount of CH<sub>3</sub>I observed at 17–18 km (0.01 ppt) simulating a too strong CH<sub>3</sub>I entrainment. However, the model results underestimate CH<sub>3</sub>I at 19 km which is suggested to be around 0.02 ppt according to observations. Since CH<sub>3</sub>I has no source in the atmosphere one would expect to find lower values at higher altitudes. A horizontally moving aircraft, however, will probe different air masses at the different altitude levels and a positive vertical gradient as noted between 17 and 19 km can occur. The overall comparison of the 17–19 km region gives a good agreement between observations (0.011–0.019 ppt) and model results (0.006–0.032 ppt).

### 4.3 Global CH<sub>3</sub>I in the upper TTL

It is also of interest to estimate CH<sub>3</sub>I abundances in regions where no in-situ measurements in the upper TTL are available. The projected amount of CH<sub>3</sub>I entrained into the stratosphere depends on various FLEXPART model parameters and their associated uncertainties such as uncertainties in the convective parameterization and in the vertical transport driven by the vertical wind fields. The accurate representation of convection has been validated with tracer experiments and <sup>222</sup>Rn measurements (Forster et al., 2007). The application of transport timescales based on vertical heating rates instead of vertical wind fields in the TTL between 15 and 17 km results in only minor differences of VLS entrainment (Tegtmeier et al., 2012). As discussed earlier, our results are also constrained by the prescribed CH<sub>3</sub>I lifetime which can cause variations of CH<sub>3</sub>I entrainment into the stratosphere of around 50 %. However, the overall good agreement between model and observations in the East Pacific encourages the use of the FLEXPART model results for further analysis.

The West Pacific region is of particular interest for the troposphere–stratosphere transport, and we will evaluate how the FLEXPART results in this area compare to the

## The contribution of oceanic methyl iodide to stratospheric iodine

S. Tegtmeier et al.

Title Page

Abstract

Introduction

Conclusions

References

Tables

Figures

⏪

⏩

◀

▶

Back

Close

Full Screen / Esc

Printer-friendly Version

Interactive Discussion

model results and observations in the East Pacific. Such a comparison will allow speculations of how representative existing aircraft measurements are of global estimates. In Fig. 10a observations averaged over four tropical campaigns that cross the East Pacific are displayed together with FLEXPART results averaged over three regions, the whole tropical belt (30° N–30° S), the tropical West Pacific and the tropical East Pacific aircraft campaign area. While for the West Pacific and the tropical belt the 2009 annual mean is displayed the East Pacific average is based on the months when aircraft measurements are available (see Table 3) in order to allow for a comparison of the model East Pacific mean values with the in-situ observations. The observations and model results for the East Pacific agree quite well, as discussed above for the comparisons based on coincidences. While observations suggest 0.01 ppt CH<sub>3</sub>I at 17 km the modeled profile shows slightly larger values of 0.02 ppt. Overall, the comparison indicates that the available in-situ measurements provide representative estimates of the mean CH<sub>3</sub>I abundance in the East Pacific region. FLEXPART results for the West Pacific region show considerable larger mixing ratios especially between 14 and 18 km with 0.08 ppt CH<sub>3</sub>I at 17 km. The geographical distribution of the mixing ratios is displayed on Fig. 10b indicating that the West Pacific region between 100° W and 150° E shows the largest CH<sub>3</sub>I abundances. Our model does not take into account terrestrial CH<sub>3</sub>I emissions and therefore the very-short lived CH<sub>3</sub>I is projected to reach the cold point and enter the stratosphere mostly above the oceans.

The average entrainment of CH<sub>3</sub>I into the stratosphere amounts to 0.04 ppt as demonstrated by the tropical mean (30° N–30° S) CH<sub>3</sub>I profile (Fig. 10a). In the annual mean distribution the entrainment is focused on the inner tropical latitude bands mainly between 20° S and 20° N where the mean mixing ratio is about 0.05 ppt. Figure 11 provides information on the frequency occurrence of CH<sub>3</sub>I mixing ratios at 17 km between 20° S and 20° N. As already evident from the geographical distribution in of CH<sub>3</sub>I abundances (Fig. 10) most values range between 0 and 0.1 ppt (82 %). However, a small amount of air is projected to carry larger amounts of CH<sub>3</sub>I with 5.5 % of air having mixing ratios larger than 0.2 ppt. Mixing ratios above 0.4 ppt occur only very rarely (0.6 %),







## The contribution of oceanic methyl iodide to stratospheric iodine

S. Tegtmeier et al.

Title Page

Abstract

Introduction

Conclusions

References

Tables

Figures

⏪

⏩

◀

▶

Back

Close

Full Screen / Esc

Printer-friendly Version

Interactive Discussion

Differences between existing model results can arise from different treatment of CH<sub>3</sub>I emissions, convection and photochemistry in the models. Our results show strong variations in the geographical distribution of CH<sub>3</sub>I entrainment, suggesting that currently available upper air measurements are not representative of global estimates. Further aircraft campaigns for different emission regions and especially for different convective transport regimes will be necessary in order to better understand the CH<sub>3</sub>I contribution to stratospheric iodine.

*Acknowledgements.* We thank the TransBrom, DRIVE and SHIVA team for collecting the samples and providing the oceanic VLSL measurements. The authors would also like to thank the to thank X. Zhu and L. Pope for technical support in the analysis of the whole air samples, and R. Lueb, R. Hendershot, and S. Gabbard for support of the ATTREX and HIPPO airborne sample collections. We thank Ben Miller, Steve Montzka, and Fred Moore for contributing the CH<sub>3</sub>I measurements from HIPPO2 aircraft campaign. The authors are grateful to the ECMWF for making the reanalysis product ERA-Interim available. This study is carried out within the WGL project TransBrom and the EU project SHIVA (FP7-ENV-2007-1-226224).

The service charges for this open access publication have been covered by a Research Centre of the Helmholtz Association.

## References

- Aschmann, J., Sinnhuber, B.-M., Atlas, E. L., and Schauffler, S. M.: Modeling the transport of very short-lived substances into the tropical upper troposphere and lower stratosphere, *Atmos. Chem. Phys.*, 9, 9237–9247, doi:10.5194/acp-9-9237-2009, 2009.
- Bell, N., Hsu, L., Jacob, D. J., Schultz, M. G., Blake, D. R., Butler, J. H., King, D. B., Lobert, J. M., and Maier-Reimer, E.: Methyl iodide: Atmospheric budget and use as a tracer of marine convection in global models, *J. Geophys. Res.*, 107, 4340, doi:10.1029/2001JD001151, 2002.
- Butler, J. H., King, D. B., Lobert, J. M., Montzka, S. A., Yvon-Lewis, S. A., Hall, B. D., Warwick, N. J., Mondeel, D. J., Aydin, M., and Elkins, J. W.: Oceanic distributions

**The contribution of  
oceanic methyl  
iodide to  
stratospheric iodine**

S. Tegtmeier et al.

[Title Page](#)[Abstract](#)[Introduction](#)[Conclusions](#)[References](#)[Tables](#)[Figures](#)[⏪](#)[⏩](#)[◀](#)[▶](#)[Back](#)[Close](#)[Full Screen / Esc](#)[Printer-friendly Version](#)[Interactive Discussion](#)

and emissions of short-lived halocarbons, *Global Biogeochem. Cy.*, 21, GB1023, doi:10.1029/2006GB002732, 2007.

Campos, M. L. A. M., Nightingale, P. D., and Jickells, T. D.: A comparison of methyl iodide emissions from seawater and wet depositional fluxes of iodine over the southern North Sea, *Tellus B*, 48, 106–114, doi:10.1034/j.1600-0889.1996.00010.x, 1996.

Chameides, W. L. and Davis, D. D.: Iodine: its possible role in tropospheric photochemistry, *J. Geophys. Res.*, 85, 7383, doi:10.1029/JC085iC12p07383, 1980.

Chang, C.-P., Harr, P. A., and Chen, H.-J.: Synoptic disturbances over the Equatorial South China Sea and Western Maritime Continent during boreal winter, *Mon. Weather Rev.*, 133, 489–503, doi:10.1175/MWR-2868.1, 2005.

Chipperfield, M. P.: New version of the TOMCAT/SLIMCAT off-line chemical transport model: intercomparison of stratospheric tracer experiments, *Q. J. Roy. Meteor. Soc.*, 132, 1179–1203, doi:10.1256/qj.05.51, 2006.

Chuck, A. L., Turner, S. M., and Liss, P. S.: Oceanic distributions and air-sea fluxes of biogenic halocarbons in the open ocean, *J. Geophys. Res.*, 110, C10022, doi:10.1029/2004JC002741, 2005.

Davis, D., Crawford, J., Liu, S., McKeen, S., Bandy, A., Thornton, D., Rowland, F., and Blake, D.: Potential impact of iodine on tropospheric levels of ozone and other critical oxidants, *J. Geophys. Res.*, 101, 2135, doi:10.1029/95JD02727, 1996.

Dee, D. P., Uppala, S. M., Simmons, A. J., Berrisford, P., Poli, P., Kobayashi, S., Andrae, U., Balmaseda, M. A., Balsamo, G., Bauer, P., Bechtold, P., Beljaars, A. C. M., van de Berg, L., Bidlot, J., Bormann, N., Delsol, C., Dragani, R., Fuentes, M., Geer, A. J., Haimberger, L., Healy, S. B., Hersbach, H., Hólm, E. V., Isaksen, L., Kållberg, P., Köhler, M., Matricardi, M., McNally, A. P., Monge-Sanz, B. M., Morcrette, J.-J., Park, B.-K., Peubey, C., de Rosnay, P., Tavolato, C., Thépaut, J.-N., and Vitart, F.: The ERA-Interim reanalysis: configuration and performance of the data assimilation system, *Q. J. Roy. Meteor. Soc.*, 137, 553–597, doi:10.1002/qj.828, 2011.

Dix, B., Baidar, S., Bresch, J. F., Hall, S. R., Schmidt, K. S., Wang, S., and Volkamer, R.: Detection of iodine monoxide in the tropical free troposphere, *P. Natl. Acad. Sci. USA*, 110, 2035–40, doi:10.1073/pnas.1212386110, 2013.

Donner, L. J., Horowitz, L. W., Fiore, A. M., Seman, C. J., Blake, D. R., and Blake, N. J.: Transport of radon-222 and methyl iodide by deep convection in the GFDL Global Atmospheric Model AM2, *J. Geophys. Res.*, 112, D17303, doi:10.1029/2006JD007548, 2007.

## The contribution of oceanic methyl iodide to stratospheric iodine

S. Tegtmeier et al.

Title Page

Abstract

Introduction

Conclusions

References

Tables

Figures

⏪

⏩

◀

▶

Back

Close

Full Screen / Esc

Printer-friendly Version

Interactive Discussion



- Forster, C., Wandinger, U., Wotawa, G., James, P., Mattis, I., Althausen, D., Simmonds, P., O'Doherty, S., Jennings, S. G., Kleefeld, C., Schneider, J., Trickl, T., Kreipl, S., Jäger, H., and Stohl, A.: Transport of boreal forest fire emissions from Canada to Europe, *J. Geophys. Res.*, 106, 22887, doi:10.1029/2001JD900115, 2001.
- 5 Forster, C., Stohl, A., and Seibert, P.: Parameterization of convective transport in a Lagrangian particle dispersion model and its evaluation, *J. Appl. Meteorol. Clim.*, 46, 403–422, doi:10.1175/JAM2470.1, 2007.
- Fueglistaler, S., Dessler, A. E., Dunkerton, T. J., Folkins, I., Fu, Q., and Mote, P. W.: Tropical tropopause layer, *Rev. Geophys.*, 47, RG1004, doi:10.1029/2008RG000267, 2009.
- 10 Fuhlbrügge, S., Krüger, K., Quack, B., Atlas, E., Hepach, H., and Ziska, F.: Impact of the marine atmospheric boundary layer on VLSL abundances in the eastern tropical and subtropical North Atlantic Ocean, *Atmos. Chem. Phys. Discuss.*, 12, 31205–31245, doi:10.5194/acpd-12-31205-2012, 2012.
- Gettelman, A., Lauritzen, P. H., Park, M., and Kay, J. E.: Processes regulating short-lived species in the tropical tropopause layer, *J. Geophys. Res.*, 114, D13303, doi:10.1029/2009JD011785, 2009.
- Happell, J. D. and Wallace, D. W. R.: Methyl iodide in the Greenland/Norwegian Seas and the tropical Atlantic Ocean: evidence for photochemical production, *Geophys. Res. Lett.*, 23, 2105–2108, doi:10.1029/96GL01764, 1996.
- 20 Hossaini, R., Chipperfield, M. P., Feng, W., Breider, T. J., Atlas, E., Montzka, S. A., Miller, B. R., Moore, F., and Elkins, J.: The contribution of natural and anthropogenic very short-lived species to stratospheric bromine, *Atmos. Chem. Phys.*, 12, 371–380, doi:10.5194/acp-12-371-2012, 2012.
- Hughes, C., Franklin, D. J., and Malin, G.: Iodomethane production by two important marine cyanobacteria: *Prochlorococcus marinus* (CCMP 2389) and *Synechococcus* sp. (CCMP 2370), *Mar. Chem.*, 125, 19–25, doi:10.1016/j.marchem.2011.01.007, 2011.
- 25 Krüger, K. and Quack, B.: Introduction to special issue: the *TransBrom Sonne* expedition in the tropical West Pacific, *Atmos. Chem. Phys. Discuss.*, 12, 1401–1418, doi:10.5194/acpd-12-1401-2012, 2012.
- 30 Krüger, K., Tegtmeier, S., and Rex, M.: Variability of residence time in the Tropical Tropopause Layer during Northern Hemisphere winter, *Atmos. Chem. Phys.*, 9, 6717–6725, doi:10.5194/acp-9-6717-2009, 2009.

**The contribution of oceanic methyl iodide to stratospheric iodine**

S. Tegtmeier et al.

[Title Page](#)[Abstract](#)[Introduction](#)[Conclusions](#)[References](#)[Tables](#)[Figures](#)[⏪](#)[⏩](#)[◀](#)[▶](#)[Back](#)[Close](#)[Full Screen / Esc](#)[Printer-friendly Version](#)[Interactive Discussion](#)

- Levine, J. G., Braesicke, P., Harris, N. R. P., Savage, N. H., and Pyle, J. A.: Pathways and timescales for troposphere-to-stratosphere transport via the tropical tropopause layer and their relevance for very short lived substances, *J. Geophys. Res.*, 112, D04308, doi:10.1029/2005JD006940, 2007.
- 5 Liss, P. S. and Slater, P. G.: Flux of gases across the air-sea interface, *Nature*, 247, 181–184, doi:10.1038/247181a0, 1974.
- Manley, S. L. and Dastoor, M. N.: Methyl halide production from the giant kelp, *Macrocystis* and estimates of global  $\text{CH}_3\text{X}$  production by kelp, *Limnol. Oceanogr.*, 32, 709–715, 1987.
- Manley, S. L. and Dastoor, M. N.: Methyl iodide ( $\text{CH}_3\text{I}$ ) production by kelp and associated mi-
- 10 crobes, *Mar. Biol.*, 98, 477–482, doi:10.1007/BF00391538, 1988.
- Manley, S. L. and De la Cuesta, J. L.: Methyl iodide production from marine phytoplankton cultures, *Limnol. Oceanogr.*, 41, 142–147, 1997.
- McFiggans, G., Plane, J. M. C., Allan, B. J., Carpenter, L. J., Coe, H., and O’Dowd, C.: A modeling study of iodine chemistry in the marine boundary layer, *J. Geophys. Res.*, 105, 14371, doi:10.1029/1999JD901187, 2000.
- 15 Montzka, S. A. and Reimann, S.: Ozone-depleting substances and related chemicals, in *Scientific Assessment of Ozone Depletion: 2010, Global Ozone Research and Monitoring Project – Report No. 52*, Geneva, Switzerland, 2011.
- Moore, R. M. and Groszko, W.: Methyl iodide distribution in the ocean and fluxes to the atmosphere, *J. Geophys. Res.*, 104, 11163, doi:10.1029/1998JC900073, 1999.
- 20 Moore, R. M. and Zafiriou, O. C.: Photochemical production of methyl iodide in seawater, *J. Geophys. Res.*, 99, 16415, doi:10.1029/94JD00786, 1994.
- Moore, R. M., Geen, C. E., and Tait, V. K.: Determination of Henry’s Law constants for a suite of naturally occurring halogenated methanes in seawater, *Chemosphere*, 30, 1183–1191, doi:10.1016/0045-6535(95)00009-W, 1995.
- 25 Murakami, H., Wang, B., and Kitoh, A.: Future change of Western North Pacific typhoons: projections by a 20-km-Mesh Global Atmospheric Model, *J. Climate*, 24, 1154–1169, doi:10.1175/2010JCLI3723.1, 2011.
- Nightingale, P. D., Malin, G., Law, C. S., Watson, A. J., Liss, P. S., Liddicoat, M. I., Boutin, J., and Upstill-Goddard, R. C.: In situ evaluation of air-sea gas exchange parameterizations using novel conservative and volatile tracers, *Global Biogeochem. Cy.*, 14, 373–387, doi:10.1029/1999GB900091, 2000.
- 30

**The contribution of  
oceanic methyl  
iodide to  
stratospheric iodine**

S. Tegtmeier et al.

Title Page

Abstract

Introduction

Conclusions

References

Tables

Figures

◀

▶

◀

▶

Back

Close

Full Screen / Esc

Printer-friendly Version

Interactive Discussion

- Ordóñez, C., Lamarque, J.-F., Tilmes, S., Kinnison, D. E., Atlas, E. L., Blake, D. R., Sousa Santos, G., Brasseur, G., and Saiz-Lopez, A.: Bromine and iodine chemistry in a global chemistry-climate model: description and evaluation of very short-lived oceanic sources, *Atmos. Chem. Phys.*, 12, 1423–1447, doi:10.5194/acp-12-1423-2012, 2012.
- 5 O'Dowd, C. D., Jimenez, J. L., Bahreini, R., Flagan, R. C., Seinfeld, J. H., Hämeri, K., Pirjola, L., Kulmala, M., Jennings, S. G., and Hoffmann, T.: Marine aerosol formation from biogenic iodine emissions, *Nature*, 417, 632–636, 2002.
- Quack, B., Atlas, E., Petrick, G., Stroud, V., Schauffler, S., and Wallace, D. W. R.: Oceanic bromoform sources for the tropical atmosphere, *Geophys. Res. Lett.*, 31, L23S05, doi:10.1029/2004GL020597, 2004.
- 10 Quack B., Atlas, E., Krüger, K., Taylor, B., Dinter, T., Bracher, A., Petrick, G., Stange, K., Fuhlbrügge, S., Tegtmeier, S., Wache, S., and Wallace, D.: Distribution and air-sea fluxes of halocarbons through the Western Pacific, *Atmos. Chem. Phys. Discuss.*, in preparation, 2013.
- 15 Rasmussen, R. A., Khalil, M. A. K., Gunawardena, R., and Hoyt, S. D.: Atmospheric methyl iodide ( $\text{CH}_3\text{I}$ ), *J. Geophys. Res.*, 87, 3086, doi:10.1029/JC087iC04p03086, 1982.
- Redeker, K. R., Wang, N.-Y., Low, J. C., McMillan, A., Tyler, S. C., and Cicerone, R. J.: Emissions of methyl halides and methane from rice paddies, *Science*, 290, 966–969, doi:10.1126/science.290.5493.966, 2000.
- 20 Richter, U. and Wallace, D. W. R.: Production of methyl iodide in the tropical Atlantic Ocean, *Geophys. Res. Lett.*, 31, L23S03, doi:10.1029/2004GL020779, 2004.
- Romps, D. M. and Kuang, Z.: Overshooting convection in tropical cyclones, *Geophys. Res. Lett.*, 36, L09804, doi:10.1029/2009GL037396, 2009.
- Rossow, W. B. and Pearl, C.: 22 year survey of tropical convection penetrating into the lower stratosphere, *Geophys. Res. Lett.*, 34, L04803, doi:10.1029/2006GL028635, 2007.
- 25 Saiz-Lopez, A., Plane, J. M. C., Baker, A. R., Carpenter, L. J., Von Glasow, R., Martín, J. C. G., McFiggans, G., and Saunders, R. W.: Atmospheric chemistry of iodine, *Chem. Rev.*, 112, 1773–804, doi:10.1021/cr200029u, 2012.
- Sander, S., Friedl, R., Barker, J., Golden, D., Kurylo, M., Wine, P., Abbatt, J., Burkholder, J., Kolb, C., Moortgat, G., Huie, R., et al.: Chemical kinetics and photochemical data for use in atmospheric studies, in: *JPL Publication 10-6*, vol. 17, JPL Publication 10-6, Jet Propulsion Laboratory, Pasadena, 2011.
- 30

## The contribution of oceanic methyl iodide to stratospheric iodine

S. Tegtmeier et al.

Title Page

Abstract

Introduction

Conclusions

References

Tables

Figures

⏪

⏩

◀

▶

Back

Close

Full Screen / Esc

Printer-friendly Version

Interactive Discussion

- Singh, H. B., Salas, L. J., and Stiles, R. E.: Methyl halides in and over the eastern Pacific (40° N–32° S), *J. Geophys. Res.*, 88, 3684, doi:10.1029/JC088iC06p03684, 1983.
- Sive, B. C., Varner, R. K., Mao, H., Blake, D. R., Wingenter, O. W., and Talbot, R.: A large terrestrial source of methyl iodide, *Geophys. Res. Lett.*, 34, L17808, doi:10.1029/2007GL030528, 2007.
- Smythe-Wright, D., Boswell, S. M., Breithaupt, P., Davidson, R. D., Dimmer, C. H., and Eiras Diaz, L. B.: Methyl iodide production in the ocean: Implications for climate change, *Global Biogeochem. Cy.*, 20, GB3003, doi:10.1029/2005GB002642, 2006.
- Solomon, S., Garcia, R. R., and Ravishankara, A. R.: On the role of iodine in ozone depletion, *J. Geophys. Res.*, 99, 20491, doi:10.1029/94JD02028, 1994.
- Spichtinger, N., Wenig, M., James, P., Wagner, T., Platt, U., and Stohl, A.: Satellite detection of a continental-scale plume of nitrogen oxides from boreal forest fires, *Geophys. Res. Lett.*, 28, 4579–4582, doi:10.1029/2001GL013484, 2001.
- Stemmler, I., Rothe, M., and Hense, I.: Numerical modelling of methyl iodide in the Eastern Tropical Atlantic, *Biogeosciences Discuss.*, 10, 1111–1145, doi:10.5194/bgd-10-1111-2013, 2013.
- Stohl, A. and Thomson, D. J.: A density correction for Lagrangian particle dispersion models, *Bound.-Lay. Meteorol.*, 90, 155–167, doi:10.1023/A:1001741110696, 1999.
- Stohl, A. and Trickl, T.: A textbook example of long-range transport: simultaneous observation of ozone maxima of stratospheric and North American origin in the free troposphere over Europe, *J. Geophys. Res.*, 104, 30445, doi:10.1029/1999JD900803, 1999.
- Stohl, A., Hittenberger, M., and Wotawa, G.: Validation of the lagrangian particle dispersion model FLEXPART against large-scale tracer experiment data, *Atmos. Environ.*, 32, 4245–4264, doi:10.1016/S1352-2310(98)00184-8, 1998.
- Stohl, A., Forster, C., Frank, A., Seibert, P., and Wotawa, G.: Technical note: The Lagrangian particle dispersion model FLEXPART version 6.2, *Atmos. Chem. Phys.*, 5, 2461–2474, doi:10.5194/acp-5-2461-2005, 2005.
- Tegtmeier, S., Krüger, K., Quack, B., Atlas, E. L., Pisso, I., Stohl, A., and Yang, X.: Emission and transport of bromocarbons: from the West Pacific ocean into the stratosphere, *Atmos. Chem. Phys.*, 12, 10633–10648, doi:10.5194/acp-12-10633-2012, 2012.
- Toon, O. B., Starr, D. O., Jensen, E. J., Newman, P. A., Platnick, S., Schoeberl, M. R., Wennberg, P. O., Wofsy, S. C., Kurylo, M. J., Maring, H., Jucks, K. W., Craig, M. S., Vasques, M. F., Pfister, L., Rosenlof, K. H., Selkirk, H. B., Colarco, P. R., Kawa, S. R., Mace, G. G.,

## The contribution of oceanic methyl iodide to stratospheric iodine

S. Tegtmeier et al.

Title Page

Abstract

Introduction

Conclusions

References

Tables

Figures

⏪

⏩

◀

▶

Back

Close

Full Screen / Esc

Printer-friendly Version

Interactive Discussion

Minnis, P., and Pickering, K. E.: Planning, implementation, and first results of the Tropical Composition, Cloud and Climate Coupling Experiment (TC4), *J. Geophys. Res.*, 115, D00J04, doi:10.1029/2009JD013073, 2010.

Vogt, R., Sander, R., Von Glasow, R., and J Crutzen, P.: Iodine chemistry and its role in halogen activation and ozone loss in the marine boundary layer?: a model study, *J. Atmos. Chem.*, 32, 375–395, 1999.

WMO (World Meteorological Organization): Scientific Assessment of Ozone Depletion: 2006, Global Ozone Research and Monitoring Project – Report No. 50, Geneva, 2007.

Wofsy, S. C., HIPPO Sci Team, Cooperating Modellers Team and Satellite Team: HIAPER Pole-to-Pole Observations (HIPPO): fine-grained, global-scale measurements of climatologically important atmospheric gases and aerosols, *Philos. T. R. Soc. A*, 369, 2073–86, doi:10.1098/rsta.2010.0313, 2011.

Yokouchi, Y., Osada, K., Wada, M., Hasebe, F., Agama, M., Murakami, R., Mukai, H., Nojiri, Y., Inuzuka, Y., Toom-Saunty, D., and Fraser, P.: Global distribution and seasonal concentration change of methyl iodide in the atmosphere, *J. Geophys. Res.*, 113, D18311, doi:10.1029/2008JD009861, 2008.

Zhou, Y., Mao, H., Russo, R. S., Blake, D. R., Wingenter, O. W., Haase, K. B., Ambrose, J., Varner, R. K., Talbot, R., and Sive, B. C.: Bromoform and dibromomethane measurements in the seacoast region of New Hampshire, 2002–2004, *J. Geophys. Res.*, 113, D08305, doi:10.1029/2007JD009103, 2008.

Ziska, F., Quack, B., Abrahamsson, K., Archer, S. D., Atlas, E., Bell, T., Butler, J. H., Carpenter, L. J., Jones, C. E., Harris, N. R. P., Hepach, H., Heumann, K. G., Hughes, C., Kuss, J., Krüger, K., Liss, P., Moore, R. M., Orlikowska, A., Raimund, S., Reeves, C. E., Reifenhäuser, W., Robinson, A. D., Schall, C., Tanhua, T., Tegtmeier, S., Turner, S., Wang, L., Wallace, D., Williams, J., Yamamoto, H., Yvon-Lewis, S., and Yokouchi, Y.: Global sea-to-air flux climatology for bromoform, dibromomethane and methyl iodide, *Atmos. Chem. Phys. Discuss.*, 13, 5601–5648, doi:10.5194/acpd-13-5601-2013, 2013.

## The contribution of oceanic methyl iodide to stratospheric iodine

S. Tegtmeier et al.

Title Page

Abstract

Introduction

Conclusions

References

Tables

Figures

⏪

⏩

◀

▶

Back

Close

Full Screen / Esc

Printer-friendly Version

Interactive Discussion

**Table 1.** Global CH<sub>3</sub>I emission estimates in the literature given in Gg I yr<sup>-1</sup> and additionally in pmol CH<sub>3</sub>I m<sup>-2</sup> h<sup>-1</sup>.

CH <sub>3</sub> I emission (Gg I yr <sup>-1</sup> )	CH <sub>3</sub> I emission (pmol CH <sub>3</sub> I m <sup>-2</sup> h <sup>-1</sup> )	Reference	Approach
241	593	Liss and Slater (1974)	Bottom up
1163	2862	Rasmussen et al. (1982)	Bottom up
270–450	665–1107	Singh et al. (1983)	Bottom up
134	330	Campos et al. (1996)	Bottom-up
254	625	Moore and Groszko (1999)	Bottom up
272	670	Bell et al. (2002)	Top-down
180	443	Chuck et al. (2005)	Bottom up
531	1307	Smythe-Wright et al. (2006)	Lab-experiment
550	1354	Butler et al. (2007)	Bottom-up
304	748	Ordóñez et al. (2012)	Top-down
184	453	Ziska et al. (2013)	Bottom-up

## The contribution of oceanic methyl iodide to stratospheric iodine

S. Tegtmeier et al.

Title Page

Abstract

Introduction

Conclusions

References

Tables

Figures



Back

Close

Full Screen / Esc

Printer-friendly Version

Interactive Discussion



**Table 2.** Recent ship campaigns providing oceanic and atmospheric CH<sub>3</sub>I measurements.

Campaign (R/V)	Full name	Route	Time period	References
TransBrom-Sonne ( <i>Sonne</i> )	Very short lived bromine compounds in the ocean and their transport pathways into the stratosphere – <i>Sonne</i>	West Pacific: Tomakomai, Japan – Townsville, Australia	Oct 2009	Krüger and Quack (2012)
DRIVE ( <i>Poseidon</i> )	Diurnal and Regional Variability of Halogen Emissions	Atlantic: Las Palmas, Spain – Vigo, Spain	May/Jun 2010	Fuhlbrügge et al. (2012)
SHIVA-Sonne ( <i>Sonne</i> )	Stratospheric Ozone: Halogen Impacts in a Varying Atmosphere – <i>Sonne</i>	West Pacific: Singapore – Manila, Philippines	Nov 2011	<a href="http://www.geomar.de/en/research/fb2/fb2-ch/projects/shiva-sonne/">http://www.geomar.de/en/research/fb2/fb2-ch/projects/shiva-sonne/</a>

## The contribution of oceanic methyl iodide to stratospheric iodine

S. Tegtmeier et al.

Title Page

Abstract

Introduction

Conclusions

References

Tables

Figures

⏪

⏩

◀

▶

Back

Close

Full Screen / Esc

Printer-friendly Version

Interactive Discussion

**Table 3.** Aircraft campaigns with CH<sub>3</sub>I measurements used in the study.

Campaign (Aircraft)	Full name	Max. altitude	Location	Time period	References
ACCENT (WB57)	Atmospheric Chemistry of Combustion Emissions Near the Tropopause	19 km	Southern US Central America	Apr, Sep 1999	<a href="http://espoarchive.nasa.gov/archive/browse/accnt">http://espoarchive.nasa.gov/archive/browse/accnt</a>
Pre-AVE (WB57)	Pre-Aura Validation Experiment	19 km	Southern US Central America	Jan–Feb 2004	<a href="http://espoarchive.nasa.gov/archive/browse/pre_ave">http://espoarchive.nasa.gov/archive/browse/pre_ave</a>
TC4 (DC 8)	Tropical Composition, Cloud and Climate Coupling	12 km	Southern US Central America	Jul–Aug 2007	Toon et al. (2010)
TC4 (WB57)	Tropical Composition, Cloud and Climate Coupling	19 km	Southern US Central America	Aug 2007	Toon et al. (2010)
HIPPO2 (HIAPER)	HIAPER Pole-to-Pole Observations 2	14 km	Pacific	Nov 2009	Wofsy et al. (2011)
ATTREX (Global Hawk)	Airborne Tropical Tropopause Experiment	19 km	East Pacific	Oct–Nov 2011	<a href="http://espo.nasa.gov/missions/attrex">http://espo.nasa.gov/missions/attrex</a>
SHIVA (Falcon)	Stratospheric ozone: Halogen Impacts in a Varying Atmosphere	14 km	West Pacific (Maritime Continent)	Nov 2011	<a href="http://shiva.iup.uni-heidelberg.de/index.html">http://shiva.iup.uni-heidelberg.de/index.html</a>

## The contribution of oceanic methyl iodide to stratospheric iodine

S. Tegtmeier et al.

**Table 4.** Correlation coefficients between CH<sub>3</sub>I emission, horizontal wind speed and vertical transport efficiency (given by the relative amount of CH<sub>3</sub>I entrained above 17 km). The coefficients are given for the complete TransBrom and SHIVA campaigns as well as for the subsets where correlations between the CH<sub>3</sub>I emissions and vertical transport efficiency have been identified (TransBrom section 1 and 2, SHIVA section 1).

Correlation coefficients for various cruise sections	TransBrom section 1	TransBrom section 2	Trans-Brom complete	SHIVA section 1	SHIVA complete
CH <sub>3</sub> I emission and horizontal wind speed	0.93	0.93	0.82	0.70	0.62
Horizontal wind speed and vertical transport	0.87	0.74	−0.29	0.73	0.49
CH <sub>3</sub> I Emission and vertical transport	0.89	0.69	−0.05	0.59	0.28

[Title Page](#)
[Abstract](#)
[Introduction](#)
[Conclusions](#)
[References](#)
[Tables](#)
[Figures](#)
[⏪](#)
[⏩](#)
[◀](#)
[▶](#)
[Back](#)
[Close](#)
[Full Screen / Esc](#)
[Printer-friendly Version](#)
[Interactive Discussion](#)

## The contribution of oceanic methyl iodide to stratospheric iodine

S. Tegtmeier et al.

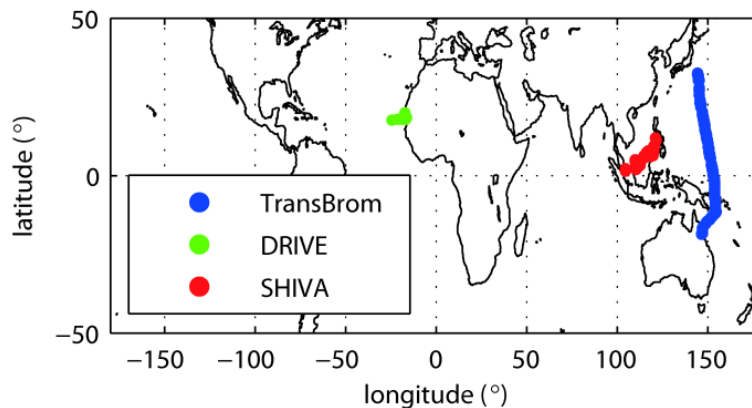


**Fig. 1.** Map of ship campaigns used in this study.

[Title Page](#)[Abstract](#)[Introduction](#)[Conclusions](#)[References](#)[Tables](#)[Figures](#)[⏪](#)[⏩](#)[◀](#)[▶](#)[Back](#)[Close](#)[Full Screen / Esc](#)[Printer-friendly Version](#)[Interactive Discussion](#)

## The contribution of oceanic methyl iodide to stratospheric iodine

S. Tegtmeier et al.

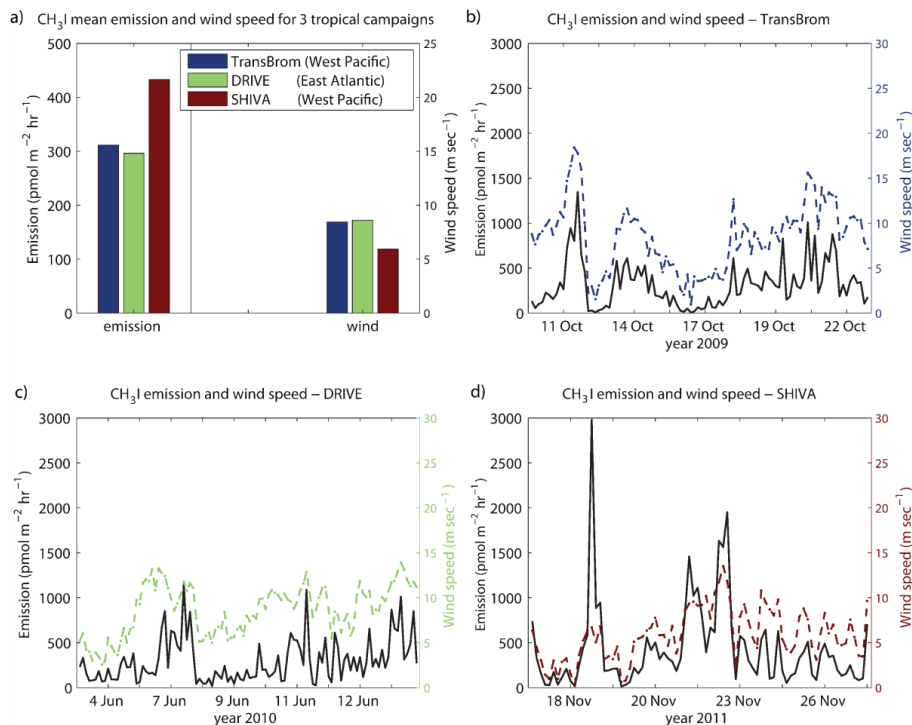


**Fig. 2.** Campaign-averaged CH<sub>3</sub>I emissions and wind speed are shown for three tropical campaigns (a). CH<sub>3</sub>I emissions (black line), as well as the wind speed (colored line) are displayed as a function of time along the cruise track for TransBrom (b), DRIVE (c), and SHIVA (d).

Title Page

Abstract

Introduction

Conclusions

References

Tables

Figures

◀

▶

◀

▶

Back

Close

Full Screen / Esc

Printer-friendly Version

Interactive Discussion

## The contribution of oceanic methyl iodide to stratospheric iodine

S. Tegtmeier et al.

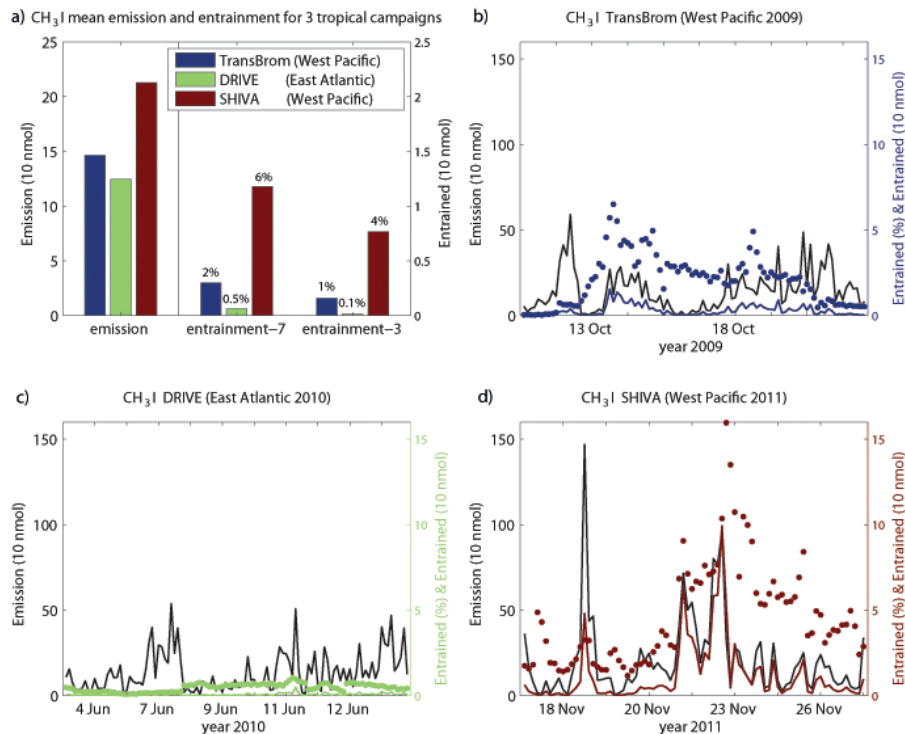


**Fig. 3.** Campaign-averaged CH<sub>3</sub>I emissions and modeled entrainment above 17 km are shown for three tropical campaigns **(a)**. CH<sub>3</sub>I emissions (black line), as well as the relative (colored dots) and total (colored line) amount of CH<sub>3</sub>I entrained above 17 km are displayed as a function of time along the cruise track for TransBrom **(b)**, DRIVE **(c)**, and SHIVA **(d)**. Emissions are calculated from the observed flux for a time period of one hour and an area of 500 m<sup>2</sup> for each observation. CH<sub>3</sub>I lifetime is prescribed with 7 days (entrainment-7 in **a** and all results in **b–d**) or with 2 ~ 3 days (entrainment-3 in **a**).

## The contribution of oceanic methyl iodide to stratospheric iodine

S. Tegtmeier et al.

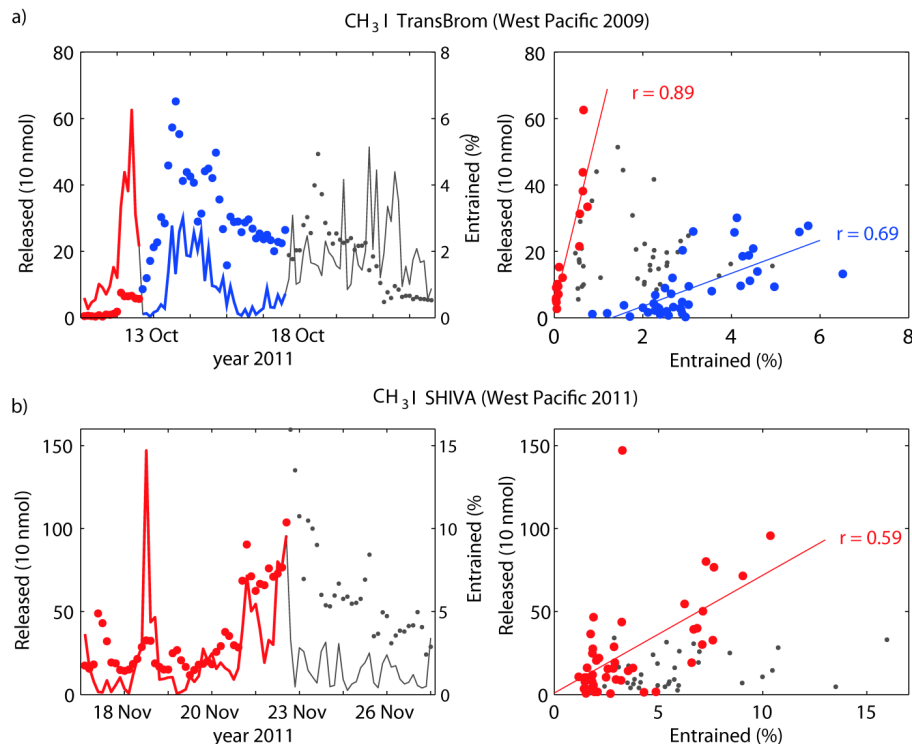


**Fig. 4.** The CH<sub>3</sub>I observed emissions (line), and the modeled relative amount entrained above 17 km (dots) are shown for TransBrom (a) and SHIVA (b) as a function of time (left panels) and as a scatter plot (right panels). The subsets, for which correlations between the two functions have been identified, are color-coded in red and blue. The correlation coefficients ( $r$ ) are given in the right panel.

## The contribution of oceanic methyl iodide to stratospheric iodine

S. Tegtmeier et al.

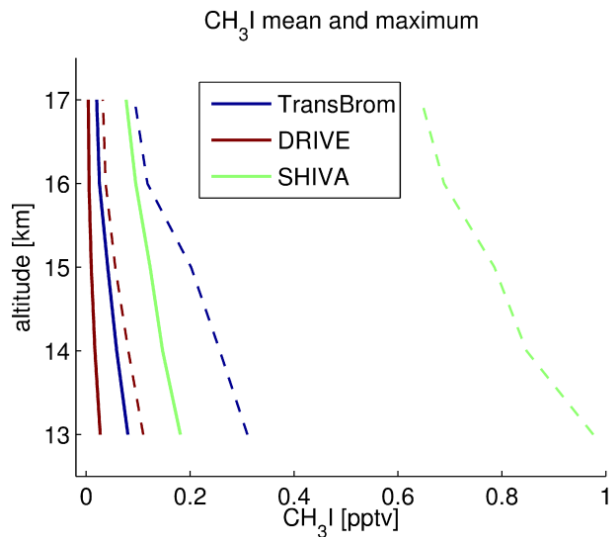


**Fig. 5.** CH<sub>3</sub>I profiles modeled based on observed emissions during the TransBrom, DRIVE and SHIVA ship campaigns. For all three campaigns mean values (solid lines) and maximum values (dashed lines) are given.

[Title Page](#)[Abstract](#)[Introduction](#)[Conclusions](#)[References](#)[Tables](#)[Figures](#)[⏪](#)[⏩](#)[◀](#)[▶](#)[Back](#)[Close](#)[Full Screen / Esc](#)[Printer-friendly Version](#)[Interactive Discussion](#)

## The contribution of oceanic methyl iodide to stratospheric iodine

S. Tegtmeier et al.

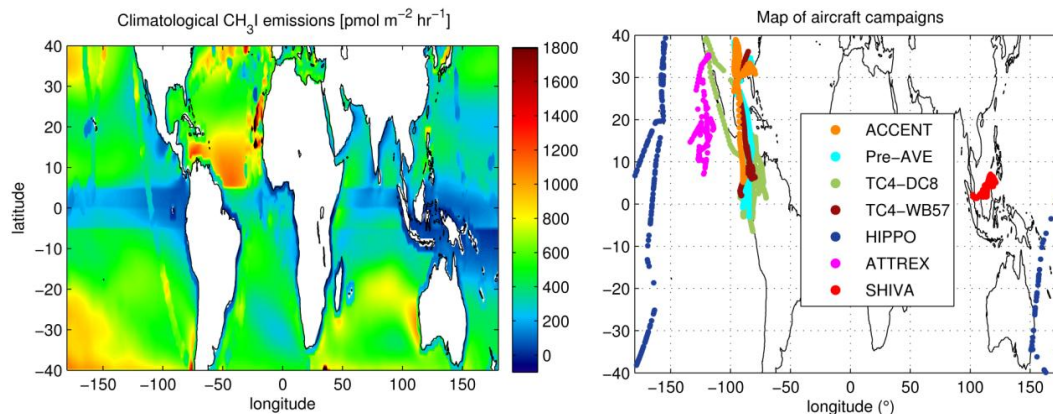


**Fig. 6.** (a) Climatological CH<sub>3</sub>I emissions [pmol m<sup>-2</sup> h<sup>-1</sup>] visualized between 40° S and 40° N on a 1° × 1° grid from Ziska et al. (2013). (b) Locations of aircraft campaign measurements for the ACCENT, Pre-AVE, TC4, HIPPO2, ATTREX, and SHIVA missions.

[Title Page](#)[Abstract](#)[Introduction](#)[Conclusions](#)[References](#)[Tables](#)[Figures](#)[⏪](#)[⏩](#)[◀](#)[▶](#)[Back](#)[Close](#)[Full Screen / Esc](#)[Printer-friendly Version](#)[Interactive Discussion](#)

## The contribution of oceanic methyl iodide to stratospheric iodine

S. Tegtmeier et al.

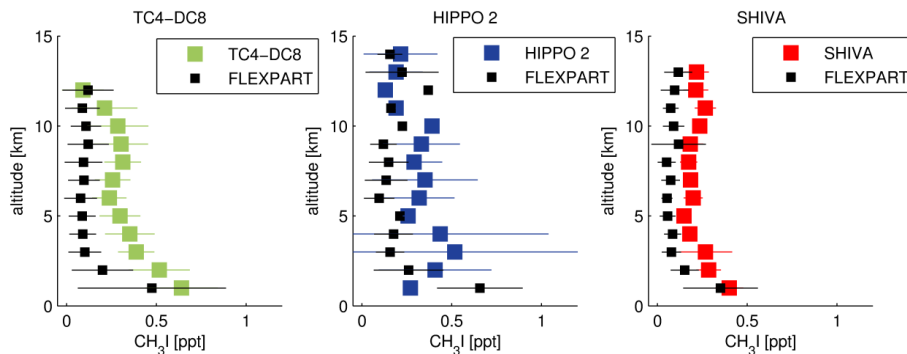


**Fig. 7.** Comparison between observed and modeled vertical profiles of  $\text{CH}_3\text{I}$  in the troposphere and lower TTL. Observations from all tropical flight sections of each aircraft campaign are used to find coincident model output. Observations and model results are averaged over all data points given in 1 km vertical intervals for TC4-DC8 (left panel), HIPPO2 (middle panel), and SHIVA (right panel). Horizontal bars indicate  $\pm 1$  standard deviation.

[Title Page](#)[Abstract](#)[Introduction](#)[Conclusions](#)[References](#)[Tables](#)[Figures](#)[◀](#)[▶](#)[◀](#)[▶](#)[Back](#)[Close](#)[Full Screen / Esc](#)[Printer-friendly Version](#)[Interactive Discussion](#)

## The contribution of oceanic methyl iodide to stratospheric iodine

S. Tegtmeier et al.

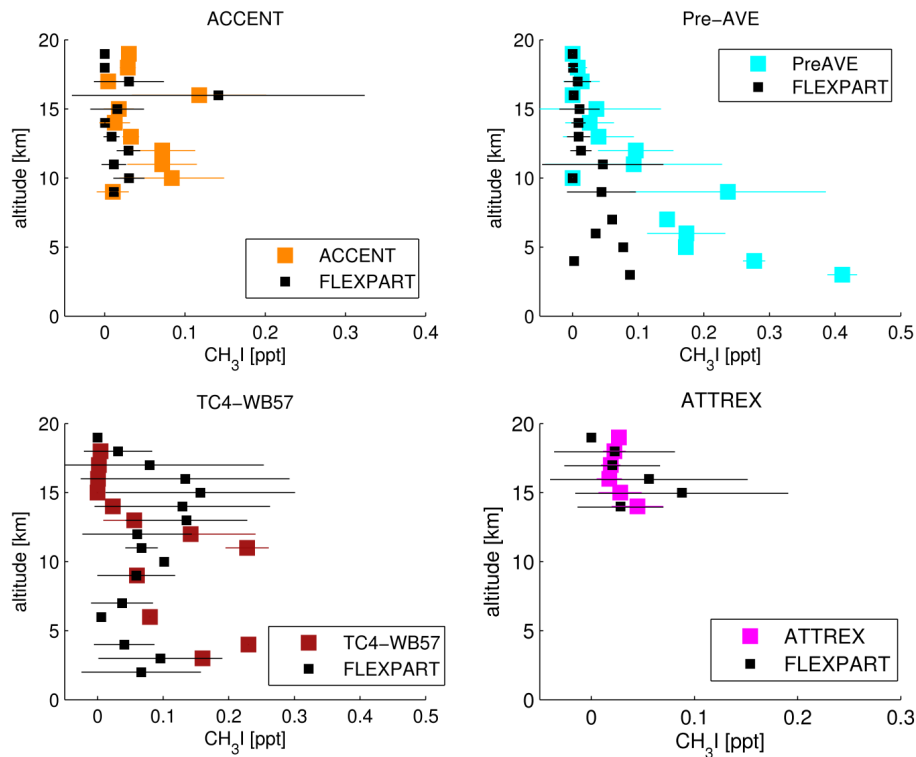


**Fig. 8.** As Fig. 7 for vertical profiles of  $\text{CH}_3\text{I}$  in the troposphere and TTL for the aircraft campaigns ACCENT, Pre-AVE, TC4-WB57, and ATTREX.

Title Page

Abstract

Introduction

Conclusions

References

Tables

Figures

⏪

⏩

◀

▶

Back

Close

Full Screen / Esc

Printer-friendly Version

Interactive Discussion

## The contribution of oceanic methyl iodide to stratospheric iodine

S. Tegtmeier et al.

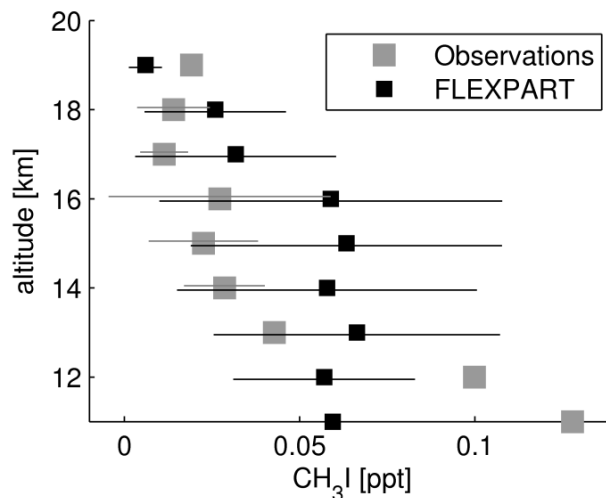


**Fig. 9.** Comparison between observed and modeled vertical profiles of  $\text{CH}_3\text{I}$  in the upper troposphere and TTL. Observations and model results are averaged over all data campaign-averaged profiles which include measurements in the upper TTL (ACCENT, Pre-AVE, TC4-WB57, and ATTREX). Horizontal bars indicate  $\pm 1$  standard deviation.

Title Page

Abstract

Introduction

Conclusions

References

Tables

Figures

⏪

⏩

◀

▶

Back

Close

Full Screen / Esc

Printer-friendly Version

Interactive Discussion

## The contribution of oceanic methyl iodide to stratospheric iodine

S. Tegtmeier et al.

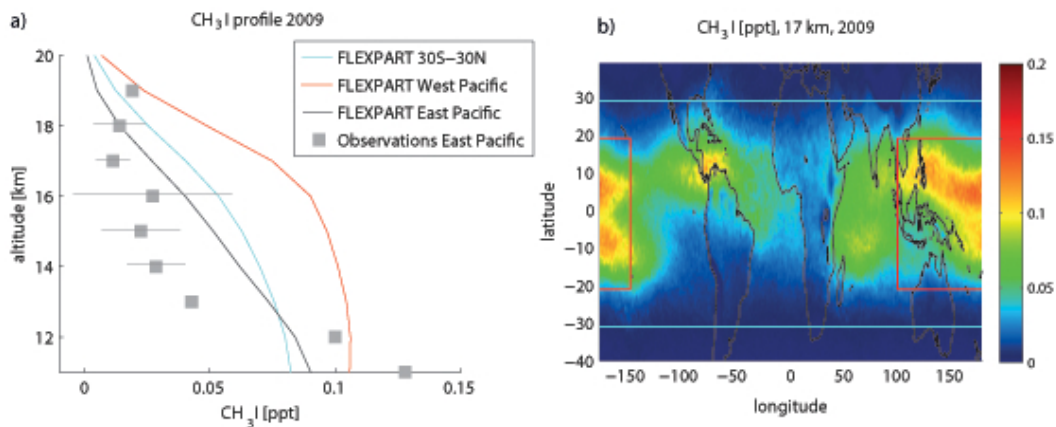


**Fig. 10.** (a) Comparison between observed and modeled vertical profiles of CH<sub>3</sub>I in the upper troposphere and TTL. Observations are as in Fig. 7. Model output is averaged over the tropics (blue, 30° S–30° N) and the West Pacific (red, 100° W–150° E, 20° S–20° N) for 2009 and the East Pacific aircraft campaign region (green, 70–130° E, 6° S–30° N) for the months of available measurements. (b) Modeled tropical distribution of CH<sub>3</sub>I at 17 km for 2009.

## The contribution of oceanic methyl iodide to stratospheric iodine

S. Tegtmeier et al.

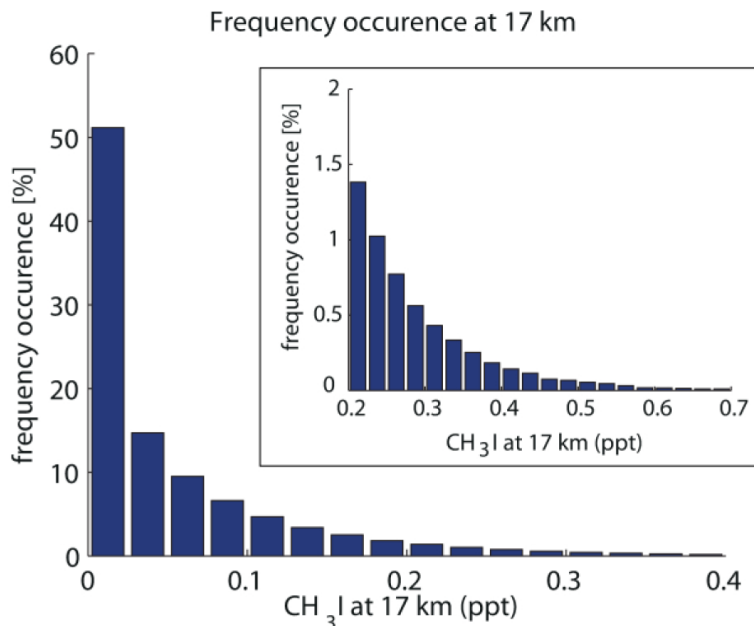


**Fig. 11.** Frequency occurrence of CH<sub>3</sub>I abundances at 17 km in the tropics for 2009 based on climatological emissions. The inset panel provides a zoom in for the range of larger mixing ratios 0.2–0.7 ppt.

[Title Page](#)[Abstract](#)[Introduction](#)[Conclusions](#)[References](#)[Tables](#)[Figures](#)[⏪](#)[⏩](#)[◀](#)[▶](#)[Back](#)[Close](#)[Full Screen / Esc](#)[Printer-friendly Version](#)[Interactive Discussion](#)